Article:
Rizzi, LG, Viegas, G and Auer, S orcid.org/0000-0003-0418-1745 (2022) Ligancy effects on nucleation kinetics. Journal of Chemical Physics, 157 (17). ARTN 174111. ISSN 0021-9606

https://doi.org/10.1063/5.0118306

Ligancy effects on nucleation kinetics

L. G. Rizzi,[1, a)] G. Viegas,[1] and S. Auer[2]
[1)] *Depto. de Física, Universidade Federal de Viçosa, CEP: 36570-000, Viçosa, MG, Brazil.*
[2)] *School of Chemistry, University of Leeds, Leeds, LS2 9JT, UK.*

(Dated: 7 September 2022)

Nucleation of particles into crystalline structures can be observed in a wide range of systems from metallic and metal-organic compounds to colloidal and polymeric patch particles. Here we perform kinetic Monte Carlo simulations to study the nucleation kinetics of particles with different ligancies z at constant supersaturation s. This approach allows one to determine several physico-chemical quantities as a function of s, including the growth probability $P(n)$, the critical nucleus size n^*, and the stationary nucleation rate J_s. Our numerical results are rationalized in terms of a self-consistent nucleation theory where both n^* and J_s present a non-trivial dependence on s, but which can be determined from the values of effective z-dependent parameters.

I. INTRODUCTION

Ligancy, also known as the coordination number in condensed matter physics; or functionality in polymer and colloidal physics; can be defined as the number of bonds that the individual building blocks of a substance can form with each other and/or with other chemical species. It is a microscopic feature of the individual particles that is intrinsically related to the collective phase behaviour of the corresponding solution; and it can be used to infer important physico-chemical properties, *e.g.* solubilities and latent heats of solidification, of many substances[1].

The self-assembly of particles with controlled ligancy is of particular interest to the design of novel materials with tailored responses. For instance, recent experiments have shown that a class of metal-organic compounds with different architectures has emerged as promising and versatile systems with potential applications in coatings, optics, photovoltaics, and magnetism[2]. However, unlike studies on the equilibrium phase diagrams of patch-interacting particles, the effects of ligancy on self-assembly kinetics are still poorly explored[3,4].

Here we perform a numerical study to investigate the effects of different ligancies z on the nucleation kinetics and develop a theoretical framework to rationalize their influence on the critical nucleus size n^* and on the stationary nucleation rate J_s as a function of the supersaturation s.

II. MODEL AND SIMULATIONS

As shown in Fig. 1, our model is defined by particles with different ligancies z which form clusters in two dimensions ($d = 2$). In addition to the particles that present one-particle unit cells with $z = 4$ and $z = 6$, we include two kinds of particles (*i.e.*, isomers or polymorphs) with $z = 5$, that nucleate into crystals which display unit cells with more than one particle. Those particles resemble motifs observed not only in experiments with metal-organic coordination networks[2,5], and in binary mixtures of nanoparticles[6]; but also in simulations on star-like patch particles with five-fold symmetry[7,8].

In order to perform kinetic Monte Carlo (KMC) simulations, we consider a system that is similar to one implemented in early studies[9–12], where there is only one cluster with n particles, so that either a particle (from an implicit bath) could attach to it or a particle that belongs to the cluster could detach from it and go to the solution (which maintains a constant supersaturation s). The microscopic attachment and detachment frequencies can be written[9,10], respectively, as $k^+(C_1) = k^+_{\rm ref} C_1$ and $k^-(b_i) = k^-_{\rm ref} \exp(-2b_i\omega)$, where C_1 is the concentration of (isolated) particles in solution, b_i is the number of neighbours connected to the i-th particle that belongs to the cluster, and $\omega = \varepsilon/2k_BT$ is the ratio between the effective binding energy[13] $\varepsilon > 0$ and the thermal energy (k_B is the Boltzmann's constant and T is the absolute temperature). The factor in the exponential of $k^-(b_i)$ is related to the work $W(b_i) = b_i\varepsilon = 2b_i\omega k_BT$ required to detach a particle from the surface of the cluster[14]. It is assumed that $k^+_{\rm ref}$ is a reference frequency which does not depend on the value of the ligancy z, while $k^-_{\rm ref}$ is a reference frequency which does not depend on the supersaturation s, which is defined as $s = \ln(C_1/C_e)$, with C_e being the solubility of the particles in solution.

At equilibrium, $C_1 = C_e$, then the equilibrium frequency can be defined as $k_e = k^+(C_e) = k^+_{\rm ref} C_e$, so that the attachment frequency can be rewritten as[9]

$$k^+(s) = k_e \exp(s) \quad . \tag{1}$$

The equilibrium condition between the cluster and the particles at solution should also ensures that $s = 0$, and that the attachment and detachment frequencies are equal, *i.e.*, $k^-(b^*_z) = k^+(0)$, where b^*_z is determined by the average number of bonds of the particles at the surface of the cluster, which can be estimated by $b^*_z = (z-1)^{-1}\sum_{i=1}^{z-1} i = z/2$. The equilibrium condition leads to $k^-_{\rm ref} = k_e \exp(2b^*_z\omega)$, so that the detachment frequency can be rewritten as

$$k^-(b_i) = k_e \exp[-2\omega(b_i - z/2)] \quad . \tag{2}$$

[a)] Corresponding author: lerizzi@ufv.br

Equations 1 and 2 allow us to implement the KMC simulations by using the same procedure established in previous studies[9–12]. In summary, for a given configuration of the cluster with n particles, one must list all the l_n^+ attachment and n detachment events that can occur, then the j-th event is randomly selected so that the configuration is modified according to attachment and detachment probabilities defined, respectively, as

$$p^+ = \frac{k^+}{l_n^+ k^+ + \sum_{i=1}^{n} k^-(b_i)} \tag{3}$$

and

$$p_j^- = \frac{k^-(b_j)}{l_n^+ k^+ + \sum_{i=1}^{n} k^-(b_i)} \quad , \tag{4}$$

with k^+ given by Eq. 1 and $k^-(b_i)$ by Eq. 2, so that the probabilities do not depend on the frequency k_e.

Our analysis starts by considering the growth probabilities, which can be defined as[12] $P(n) = N(n_c)/N(n)$, where $N(n)$ is the number of runs that grow to a cluster with n particles, and $N(n_c)$ is the total number of runs that reached a size n_c. For all simulations, we take the initial growth condition as a single particle ($n = 1$), and consider that the cluster will form a macroscopic crystal if its size reaches, at least, $n_c = 200$ particles. In order to have reasonable statistics, we evaluate $P(n)$ from simulations where at least 10^3 successful runs in which the cluster reached n_c particles (*e.g.*, we run at least 10^7 runs for simulations where $P(1) \approx 10^{-4}$).

In Fig. 1 we illustrate the growth probabilities $P(n)$ obtained for the particles with different z for $\omega = 1$. For all kinds of particles, the curves display the same qualitative behaviour, with $P(n)$ displaying a more noticeable sigmoidal-like shape when the supersaturation s is lowered (rightmost curves). Figures 1(a) and (b) show that there is a distinct behaviour for the particles with $z = 6$ and $z = 4$. At the same supersaturation s, the growth probabilities $P(n)$ indicate that a system formed by particles with higher ligancy ($z = 6$) needs to grow to larger cluster sizes in order to reach n_c, and thus a macroscopic cluster size. Interestingly, the results in Figs. 1(c) and (d) for the two kinds of particles (*i.e.*, isomers or polymorphs) with $z = 5$ indicate that, although they present the same ligancy, the difference between their shapes is sufficient to change their nucleation kinetics.

In order to further characterize the nucleation of the different particles, we evaluate the critical nucleus size n^*, which is determined numerically from the inflection point of the growth probability $P(n)$. As illustrated in the inset of Fig. 1(b) for $z = 4$, this is done by considering a fit of the numerical data to the derivative of the approximated function[15]

$$P(n) = \frac{\mathrm{erf}[\nu(n - n^*)] + \mathrm{erf}[\nu(n^* - 1)]}{1 + \mathrm{erf}[\nu(n^* - 1)]} \quad , \tag{5}$$

where $\mathrm{erf}(x)$ is the error function and ν is a free parameter which can be related to the Zeldovich factor[16]. As shown in Fig. 1(b), the derivative of expression 5 fits the numerical data well when $P(n)$ displays a sigmoidal-like curve. However, for non-sigmoidal curves the fitting procedure becomes poor, and we then estimate n^* from the condition where the growth probability is $P(n^*) = 0.5$, as in Ref.[12] (if $P(1) > 0.5$ we just assume $n^* = 1$).

The evaluation of the growth probability curves $P(n)$ also allow us to determine the one-component station-

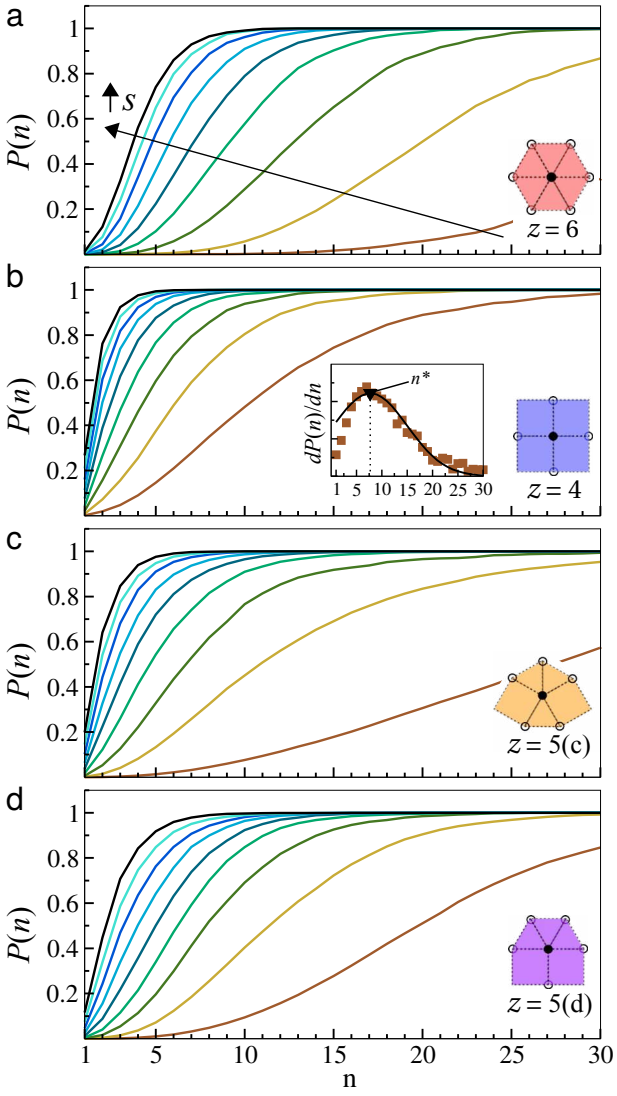

FIG. 1. Growth probabilities $P(n)$ for particles with different z for $\omega = 1$. (a) and (b) show particles with ligancies equal to $z = 6$ and $z = 4$, respectively; (c) and (d) display the two kinds of particles (*i.e.*, isomers or polymorphs) that have $z = 5$. From right to left the different curves indicate increasing values of the supersaturation s: 0.4, 0.6, 0.8, 1, 1.2, 1.4, 1.6, 1.8, and 2. Inset panel in (b) illustrates the determination of n^* for $z = 4$ and $s = 0.4$ through the derivative of $P(n)$: filled squares denote the numerical data while the continuous line denotes the fit to a Gaussian function obtained from expression 5.

ary nucleation rate $J_s = J_s(s)$, which gives the number of clusters of size $n > n^*$ that are steadily nucleated per unit of time and per unit of volume, in the supersaturated old phase. As discussed in Refs.[9,11,15], J_s can be conveniently evaluated from the dimer growth probability $P(2)$, that is, $J_s = f_1 C_1 P(2)$, where f_1 is the monomer-to-monomer attachment frequency. We note that all simulations start with $n = 1$ particles in order to avoid biases in the evaluation of $P(2)$ caused by any specific choice of a dimer configuration, specially in the case of the isomers with $z = 5$.

III. RESULTS

As discussed in Ref.[13] for $z = 4$, the behaviour of $J_s(s)$ and $n^*(s)$ can be qualitatively different depending on the the value of ω, so we first include results for the case of weak interacting particles where $\omega = 1.4$, and later for the case where $\omega = 3$. Nevertheless, we show that both cases can be well described by the same theoretical framework developed here.

For $\omega = 1.4$, in particular, Fig. 2(a) shows that there is a common qualitative behaviour for all z with $n^*(s)$ decreasing as the supersaturation s increases. Also, it shows that the smaller the ligancy, the smaller the value of n^*. Figure 2(b) shows that the reduced stationary rate $\bar{J}(s) = J_s/f_1 C_1$ presents a behaviour that is opposite but consistent to what is observed for the critical nucleus size $n^*(s)$, where $\bar{J}(s)$ displays larger values for smaller ligancies, with the curves for $z = 5$ presenting intermediary values between $z = 4$ and $z = 6$. As illustrated in the linear plot presented in inset of Fig. 2(b), the curves for the reduced nucleation rate $\bar{J}(s)$ present a similar sigmoidal-like behaviour for all z, with the curve for $z = 6$ being the one which saturates at the largest values of s.

Now, in order to obtain expressions for $n^*(s)$ and $\bar{J}(s)$ which are general enough to incorporate the ligancy effects that are observed even for the isomers with the same z, we adopt a Zeldovich-like approach, and assume n as a continuous variable[16]. In that case, we demonstrate in Appendix A that the reduced stationary rate can be estimated as

$$\bar{J}(s) = \frac{1}{1 + r(s)} \quad , \tag{6}$$

with

$$\begin{aligned} r(s) &\approx f_1 C_1 \int_2^{M_z} \frac{dn}{f(n) C(n)} \\ &\approx \upsilon_z \left(\frac{\pi}{s}\right)^{1/2} \exp\left(s - 2z\psi\beta_z + \frac{(z\psi\beta_z)^2}{s}\right) \\ &\times \left[\mathrm{erf}\left(\frac{s\sqrt{M_z} - z\psi\beta_z}{s^{1/2}}\right) - \mathrm{erf}\left(\frac{s\sqrt{2} - z\psi\beta_z}{s^{1/2}}\right)\right], \end{aligned} \tag{7}$$

where β_z, υ_z, and M_z are z-dependent parameters that are assumed to be independent of the supersaturation s,

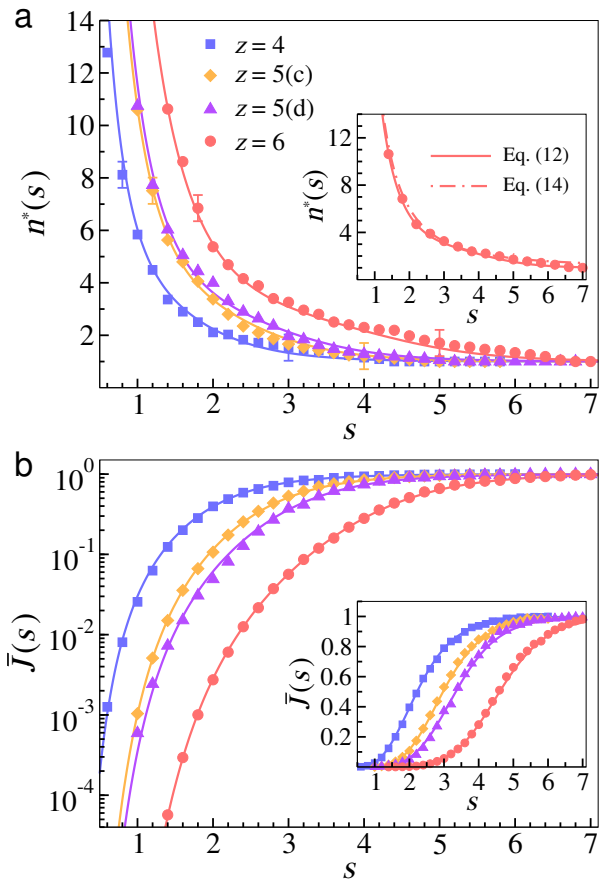

FIG. 2. (a) Critical nucleus size $n^*(s)$, and (b) reduced stationary nucleation rate $\bar{J}(s) = J_s/f_1 C_1$, obtained for particles with different ligancies z with $\omega = 1.4$. Filled symbols correspond to numerical results extracted from KMC simulations, while continuous lines denote the best fit to the z-dependent expressions: $\bar{J}(s)$ is given by Eq. 6 with $r(s)$ given by Eq. 7, and $n^*(s)$ is evaluated directly from $\bar{J}(s)$ through Eq. 12 with the derivative of $r(s)$ given by Eq. 13. Inset panel in (a) includes a comparison between Eq. 12 and the approximated expression, Eq. 14, for $z = 6$. The inset panel in (b) shows just the linear plot of the data displayed in the main panel. The parameters β_z and υ_z obtained from the fitting procedure considering $M_z = n_c$ are displayed in Table I. Error bars in (a) are used just to indicate the deviation of a half of a unit.

and $\psi = \sigma/k_B T$ is related to the effective surface energy per particle[13,17] σ, and is roughly proportional to the ratio ω defined in KMC simulations (see Appendix B). As detailed in Appendix A, M_z denotes a characteristic size which is determined by the asymptotic limit for which the growth probability $P(n)$, Eq. A1, tends to 1; υ_z is a dimensionless parameter used to define the solubility C_e (see Eq. A3), which, as discussed in Ref.[18], might be related to the ligancy z but should not depend on ψ; the parameter β_z is related to the function $l(n)$ which describes the number of non-connected bonds at the periphery of the cluster. As discussed in Ref.[13], the specific behaviour of this function is crucial in obtaining Eq. 7, as it is used to define both the attachment frequency $f(n)$ of

ω	z	$\psi\beta_z$	υ_z	M_z	ψ
1.4	4	0.565 (10)	2.1 (3)	200	0.87 (4)
1.4	5(c)	0.639 (16)	2.3 (5)	200	0.86 (5)
1.4	5(d)	0.636 (15)	5.0 (5)	200	0.88 (5)
1.4	6	0.755 (6)	6.0 (5)	200	0.91 (4)
3	4	1.719 (22)	2.1 (3)	6.9 (3)	2.64 (12)
3	5(c)	1.952 (38)	2.3 (5)	3.8 (1)	2.64 (12)
3	5(d)	1.906 (18)	5.0 (5)	3.4 (1)	2.65 (10)
3	6	2.177 (15)	6.0 (5)	2.7 (3)	2.63 (9)

TABLE I. z-dependent values determined from the fit of Eq. 6 to the numerical estimates of $\bar{J}(s)$ obtained from the KMC simulations and presented in Fig. 2(b) for $\omega = 1.4$, and in Fig. 3 for $\omega = 3$. The values of ψ in the last column were obtained from the product $\psi\beta_z$ (third column) by considering the values of β_z extracted from the data displayed in Fig. 4. The values inside the parentheses indicate rough estimates of the maximum deviations that can be made in the last digits that do not significantly alter the numerical fit.

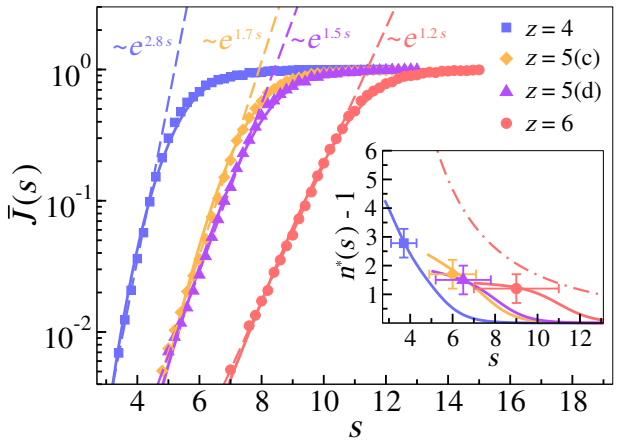

FIG. 3. Reduced stationary nucleation rate $\bar{J}(s) = J_s/f_1C_1$ (main panel) for particles with different ligancies z and for $\omega = 3$. Filled symbols correspond to results extracted from KMC simulations, while continuous lines denote the best fit of the numerical data to the z-dependent expression for $\bar{J}(s)$ given by Eq. 6 with $r(s)$ given by Eq. 7. Continuous lines in the inset panel denote $n^*(s) - 1$, with the critical nucleus size evaluated from $\bar{J}(s)$ through Eq. 12 with the derivative of $r(s)$ given by Eq. 13 using the parameters β_z, υ_z, and M_z, that are listed in Table I. Filled symbols and horizontal error bars in the inset panel denote, respectively, the values of $n^* - 1$ and the validity ranges that were estimated from the fits of the data to exponential functions, *i.e.*, $\propto e^{(n^*-1)s}$, which are displayed as dashed lines in the main panel. Dash-dotted line in the corresponds to $n^*(s) - 1$ with the critical nucleus size $n^*(s)$ given by Eq. 14 for $z = 6$.

particles to a n-sized cluster, and the equilibrium cluster concentration (for $n > 1$)

$$C(n) = C_0\, e^{-w(n)} \quad , \tag{8}$$

where $w(n)$ is the dimensionless work to form a cluster with n particles, and $C_0 = 1/v_0$, so that v_0 sets a characteristic length $\ell = v_0^{1/3}$ related to the size of a monomeric particle which can be used to define the physical units for the concentrations and for the solubility C_e (see Eq. A3). As detailed in Appendix B, we assume that the above mentioned quantities are given by (see Eq. B5)

$$f(n) = f_1 l(n)/z = f_1 \left[1 + 2\beta_z(n^{1/2} - 1)\right] \quad , \tag{9}$$

and (see Eq. B6)

$$w(n) = -sn + \psi l(n) = -sn + 2z\psi\beta_z(n^{1/2} - 1) + z\psi \ , \tag{10}$$

where the exponent $\alpha = 1/2$ is chosen because the model is defined in two-dimensions. It is worth noting that the value $\beta_z = 1/2$ leads Eqs. 9 and 10 to be the somewhat expected expressions for the regular lattice with $z = 4$, *i.e.*, a two-dimensional Kossel crystal (see Ref.[13] and Appendix B). However, as the numerical results displayed in Fig. 2 suggest, different values for β_z should be considered if one aims to describe the different behaviours that are observed for the isomers with $z = 5$.

In order to validate our theoretical approach, we first consider Eq. 6 to analyse the data obtained for $\bar{J}(s)$ with $\omega = 1.4$ that are displayed in Fig. 2(b). To do so, we assume that $M_z = n_c$, so that the first error function in Eq. 7 tends to 1 and our expression for $\bar{J}(s)$ is left with just "two" free parameters: $\psi\beta_z$ and υ_z (*i.e.*, the product $\psi\beta_z$ can be thought as a single parameter). Figure 2(b) indicates that there is a remarkable agreement between the numerical data extracted from the KMC simulations and the best fit using Eq. 6. As shown in Table I, higher ligancies z lead to higher values of $\psi\beta_z$ and υ_z. Interestingly, the values of $\psi\beta_z$ found for the isomers with $z = 5$ are very close to each other. Hence, the slightly differences observed in Fig. 2 for $z = 5$ can be associated to the values of υ_z, with the isomer with $z = 5$(d) displaying values of υ_z closer to the values found for the particle with ligancy $z = 6$.

It is worth mentioning that, although there is some freedom granted by a fitting procedure involving a function either with two or three parameters (*i.e.,* including M_z as a free parameter), we did it in a way that the values of $\bar{J}(s)$ also provide a consistent description for the numerically determined values of critical nucleus sizes n^* displayed in Fig. 2(a). In order to do that in a consistent way, we first assume that the stationary nucleation rate can be written as $J_s = Ae^{-w^*}$, with the pre-factor A being independent of the supersaturation, and with $w^* = w^*(s)$ being the work to form the critical nucleus. Hence, by recalling that $J_s = f_1C_1\bar{J}$ with $C_1 = C_e e^s$, one can invert the relationship between J_s and w^* and compute the critical nucleus size $n^*(s)$ through the so-called nucleation theorem[16], which establishes that

$$n^*(s) = -\frac{dw^*}{ds} \approx 1 + \frac{d\ln[\bar{J}(s)]}{ds} \quad . \tag{11}$$

Thus, by assuming that the reduced stationary nucleation rate $\bar{J}(s)$ is given by Eq. 6, one can rewrite the

above equation as

$$n^*(s) \approx 1 - \frac{1}{1+r(s)}\frac{dr(s)}{ds} \quad , \tag{12}$$

with the derivative of the function $r(s)$, Eq. 7, given by

$$\begin{aligned}\frac{dr(s)}{ds} &= r(s) + v_z \exp\left(s - 2z\psi\beta_z + \frac{(z\psi\beta_z)^2}{s}\right) \\ &\times \left\{\left(\frac{s\sqrt{M_z} + z\psi\beta_z}{s^2}\right)\exp\left(-\frac{(s\sqrt{M_z} - z\psi\beta_z)^2}{s}\right)\right. \\ &- \left(\frac{s\sqrt{2} + z\psi\beta_z}{s^2}\right)\exp\left(-\frac{(s\sqrt{2} - z\psi\beta_z)^2}{s}\right) \\ &- \left(\frac{\pi}{s}\right)^{1/2}\left(\frac{1}{2s} + \frac{(z\psi\beta_z)^2}{s^2}\right)\left[\mathrm{erf}\left(\frac{s\sqrt{M_z} - z\psi\beta_z}{s^{1/2}}\right)\right. \\ &- \left.\left.\mathrm{erf}\left(\frac{s\sqrt{2} - z\psi\beta_z}{s^{1/2}}\right)\right]\right\} \quad . \end{aligned} \tag{13}$$

Figure 2(a) shows that, although in a non-trivial manner, the critical nucleus size $n^*(s)$ evaluated through Eqs. 12 and 13 lead to a remarkable agreement with the numerical data extracted from the KMC simulations. Alternatively, one can use the condition of maximum work[13], $(dw(n)/dn)_{n=n^*-1} = 0$, with $w(n)$ given by Eq. 10, to obtain an approximated (but simpler) expression for the critical nucleus size, that is

$$n^*(s) = \frac{(z\psi\beta_z)^2}{s^2} + 1 \quad . \tag{14}$$

Indeed, as illustrated in the inset of Fig. 2(a), Eq. 14 can be used with the same parameters listed in Table I to provide a good description of the numerical data obtained for $\omega = 1.4$, just like the lengthy expression, *i.e.*, Eq. 12 with 13. However, as we will discuss next, such simpler expression for $n^*(s)$ turned out to be inappropriate for a higher value of ω.

The results presented in Fig. 3, in particular, indicate that the numerical estimates obtained for the reduced stationary nucleation rate for $\omega = 3$ display the same trend as the results presented in Fig. 2(b), *i.e.*, the higher the ligancy z, the lower the values of $\bar{J}(s)$, however, the qualitative behaviour of $\bar{J}(s)$ curves at low supersaturation s are clearly different. As previously suggested in Ref.[13], higher values of ω may lead $\bar{J}(s)$ to display an exponential-like behaviour, where curves with nearly linear portions can be observed in a log-linear plot. As indicated by the dashed lines in Fig. 3, these regions can be identified from a fit of the numerical data to a single exponential function. Interestingly, the atomistic nucleation theory (ANT) discussed in Ref.[13] predicts that the exponential should be directly related to the critical nucleus size n^* as $\bar{J}(s) \propto e^{(n^*-1)s}$, from where one can also determine numerical estimates for n^*. Although Eq. 12 is a non-linear function which yields continuous values for $n^*(s)$, the numerical data shown in the inset of Fig. 3 indicate that, as the supersaturation s is lowered, $n^*(s)$ go to values which are in good agreement with the values we have obtained from the fit to the exponential function based on ANT. It is worth mentioning that we only found that this saturation-like behaviour occurs when we consider finite values for M_z, *i.e.*, right above n^*. The values of M_z presented in Table I for $\omega = 3$ are consistent with the step-like behaviour observed for the growth probabilities $P(n)$ in a wide range of supersaturations (data not shown) where $n^* < M_z$. This behaviour also corroborates the fact that, indeed, for higher values of ω, the estimates for the critical nucleus size $n^*(s)$ from Eq. 12 can be different from the values computed from the ap-

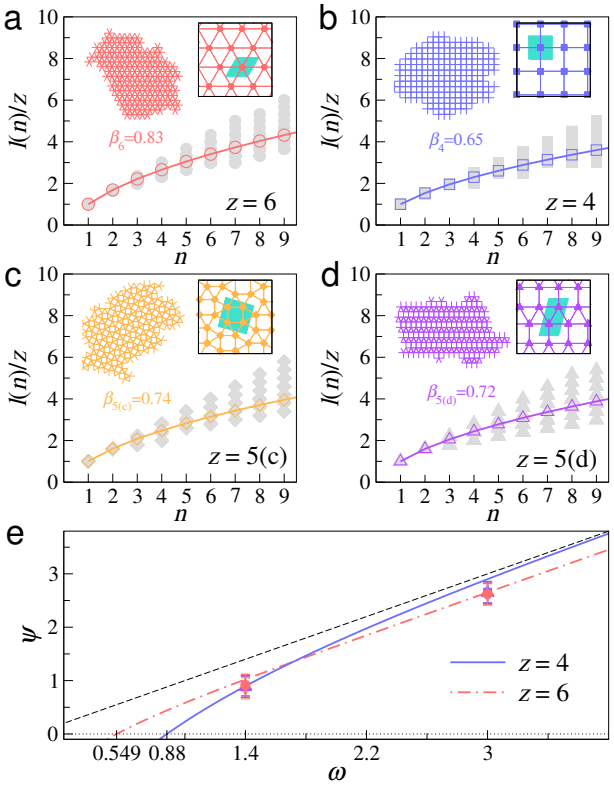

FIG. 4. Panels (a)-(d) show the normalized number of non-connected bonds at the periphery of the cluster, $l(n)/z$, for different ligancies z. Continuous lines with open symbols correspond to fit of Eq. B5 to the values averaged over several curves obtained from KMC simulations under different saturation conditions (filled grey symbols). Configurations illustrate shapes with the β_z obtained from the fit. Inset panels show zoomed in regions indicating the unit cells of each lattice (cyan). Panel (e) displays the ratio ψ between the effective surface energy per particle σ and the thermal energy k_BT as a function of the effective value ω defined in KMC simulations; filled symbols are the values listed in Table I, dashed (black) line is a reference curve $\psi = \omega$, continuous (blue) line corresponds to[13,17] $\psi = \omega + \ln[(1-e^{-\omega})/(1+e^{-\omega})]$ for $z = 4$, and dash-dotted (red) line to $\psi = \omega + 0.5\ln[(1-e^{-2\omega})/2]$ for $z = 6$ (see Ref.[19] for details). The values $\omega \approx 0.88$ and $\omega \approx 0.549$ correspond to the theoretically predicted critical ratios ω_c^z where $\psi = 0$ for $z = 4$ and $z = 6$, respectively (see Appendix B for details).

proximated expression given by Eq. 14 (as illustrated in the inset of Fig. 3).

Finally, in order to test the expression B5 that we propose for the number of non-connected bonds, we present in Fig. 4 the results for $l(n)$ obtained from KMC simulations for the different values of z. The numerical data, which were extracted from independent simulations for both values of ω and at several supersaturations s, indicate that $l(n)$ is approximately independent of ω and s (at least for small values of n). Accordingly, by considering a fit of expression B5 to the numerical data one can directly determine the values of β_z for the different ligancies z, and those can be used to estimate the values of the ratio ψ which are related to the effective surface energy per particle. The values listed in Table I indicate that the higher the ligancy z, the higher the parameter β_z, with the isomers characterized by $z = 5$ displaying similar values which are smaller than $\beta_6 = 0.83$ but higher than $\beta_4 = 0.65$. It is worth noting that, indeed, the values of ψ differ from the values of the ratio ω which are related to the effective binding energy, and the data obtained for the different ligancies yield similar values, *i.e.*, $\psi \approx 0.88$ for $\omega = 1.4$ and $\psi \approx 2.64$ for $\omega = 3$. As we indicate in Fig. 4(e), the values of ψ are in a range which is consistent with the behaviour theoretically predicted for the the two-dimensional square[13,17] and triangular[19] lattices.

IV. CONCLUDING REMARKS

In summary, we have implemented KMC simulations using simple model particles to investigate the effect of their ligancies z and isomerism on the stationary nucleation rates J_s and on the critical nucleus size n^*. The numerical results obtained from simulations allowed us to validate the theoretical framework developed here for different values of z. In particular, by considering an approximated expression for the number of non-connected bonds at the periphery of the cluster $l(n)$, Eq. B5 with $\alpha = 1/2$, we were able to determine z-dependent expressions for the concentration $C(n)$, Eq. 8, the attachment frequency $f(n)$, Eq. 9, and the (dimensionless) work $w(n)$, Eq. 10, from where z-dependent expressions for the reduced stationary nucleation rate $\bar{J}(s)$, Eq. 6, and for the critical nucleus size $n^*(s)$, Eq. 12, were evaluated. In addition, our numerical results helped us to demonstrate the validity of the nucleation theorem[16], which was used to indicate that the simpler expressions for the critical nucleus size $n^*(s)$ obtained from the condition of maximum work (*i.e.*, Eq. 14 and Eq. B7), are not valid in general, specially for larger values of ω (*i.e.*, when $\varepsilon \gg k_B T$). Interestingly, it seems that, for the larger value of ω, our expression for $\bar{J}(s)$ agreed with the numerical results in displaying an exponential-like behaviour where $n^*(s)$ is approximately constant, a result which is also corroborated by the ANT theory[13].

By validating the theoretical approach developed here, we are also generalising some of the results discussed in Ref.[13] derived specifically for the models based on the Kossel crystal (see Appendix B for details) to particles with different z, including their isomers (or polymorphs). It is worth mentioning that, at present, our approach does not provide a way to estimate the values of the parameters β_z and/or υ_z, but further developments will be focused on that issue. Even so, our z-dependent expressions helped us to clarify the role of the ratio $\psi = \sigma/k_B T$ and also its relationship to the ratio ω that is used to implement KMC simulations.

Finally, we note that, although the expressions in the main text are specific for the nucleation that occurs presumably in two-dimensions (*i.e.*, where it is assumed that $\alpha = 1/2$), we believe that the expressions presented in the Appendices for the concentration $C(n)$, Eq. A4, the number of non-connected bonds $l(n)$, Eq. B5, and the (dimensionless) work $w(n)$, Eq. B6, can be used to describe the nucleation of particles with different values of that exponent, *e.g.*, $\alpha = 2/3$, as well as other effective values observed in experiments[16,20].

ACKNOWLEDGMENTS

The authors acknowledge the insightful discussions with Prof. Dimo Kashchiev, and also the financial support from the brazilian agencies CNPq (Grant N°312999/2021-6) and FAPEMIG (Universal 2016/Process APQ-01262-16).

CONFLICT OF INTEREST

The authors have no conflicts to disclose.

APPENDIX

Appendix A: Demonstration of $r(s)$ given by Eq. 7

As mentioned in the main text, in order to obtain $r(s)$ given by Eq. 7, we consider a Zeldovich-like approach[16], and assume the size n of the cluster as a continuous variable. In that case, the growth probability can be written as[15]

$$P(n) = \bar{J}\left[1 + f_1 C_1 \int_2^n \frac{dm}{f(m)C(m)}\right] \quad , \tag{A1}$$

which is strictly valid for $n \geq 2$. Hence, since the reduced stationary nucleation rate $\bar{J}(s)$ is related to $r(s)$ through Eq. 6, one must have that

$$r(s) \approx f_1 C_1 \int_2^{M_z} \frac{dn}{f(n)C(n)} \quad , \tag{A2}$$

so that the parameter $M_z \geq 2$ is related to a characteristic size determined by the asymptotic limit for which $P(M_z) = 1$.

Here one can consider that $C_1 = C_r\, e^{-w(1)} = C_e e^{s}$, which is consistent not only with the dimensionless work $w(1) = -s + z\psi$ computed from Eq. 10, but also with the solubility given by[18,21]

$$C_e = C_r\, e^{-z\psi} \quad , \tag{A3}$$

with $C_r = \upsilon_z/\upsilon_0$, and $z\psi$ give an estimate for the latent heat of crystallization per particle (see Appendix B). Hence, the concentration $C(n)$ given by Eq. 8 can be rewritten as

$$C(n) = (C_1/\upsilon_z)\exp\{-[w(n) - w(1)]\} \quad . \tag{A4}$$

By considering the definitions 9 and 10 for $f(n)$ and $w(n)$, respectively, one can use the above relation to evaluate expression A2 as

$$\begin{aligned} r(s) &\approx \upsilon_z \int_2^{M_z} \frac{dn\, e^{w(n)-w(1)}}{1 + 2\beta_z(n^{1/2} - 1)} \\ &\approx \upsilon_z e^{s - 2z\psi\beta_z} \int_2^{M_z} \frac{dn\, e^{-sn + 2z\psi\beta_z n^{1/2}}}{1 + 2\beta_z(n^{1/2} - 1)} \quad , \end{aligned} \tag{A5}$$

which can be rewritten by setting $n = u^2$, so that

$$r(s) \approx \frac{\upsilon_z e^{s - 2z\psi\beta_z + (z\psi\beta_z)^2/s}}{\beta_z} \int_{\sqrt{2}}^{\sqrt{M_z}} \frac{du\, e^{-s(u - z\psi\beta_z/s)^2}}{1 + (1 - 2\beta_z)/(2\beta_z u)} \tag{A6}$$

Now, by considering the expansion $(1 + x_z)^{-1} = 1 - x_z + x_z^2 - \ldots$, with $x_z = (1 - 2\beta_z)/(2\beta_z u) \ll 1$, the above integral turns into a sum of integrals, *i.e.*, $\sum_{k=1}^{\infty} I_k$, with

$$I_k \approx (-1)^{k-1} \left(\frac{1 - 2\beta_z}{2\beta_z}\right)^{k-1} \int_{\sqrt{2}}^{\sqrt{M_z}} \frac{du\; e^{-s(u - z\psi\beta_z/s)^2}}{u^{k-1}} \quad . \tag{A7}$$

Unfortunately, such k-dependent integrals are not easily computed for $k \geq 2$, even so, one might approximate the sum of them by $\sum_{k=2}^{\infty} I_k \approx \kappa_z I_1$, where κ_z is a s-independent correction factor which takes into account the integrals corresponding to the higher order terms; here I_1 denotes the lowest order term (*i.e.*, for $k = 1$), which can be readily evaluated by setting $y = u - z\psi\beta_z/s$, that is,

$$\begin{aligned} I_1 &= \int_{\sqrt{2} - z\psi\beta_z/s}^{\sqrt{M_z} - z\psi\beta_z/s} dy\, e^{-sy^2} = \frac{1}{2}\left(\frac{\pi}{s}\right)^{1/2} \\ &\times \left[\mathrm{erf}\left(\frac{s\sqrt{M_z} - z\psi\beta_z}{s^{1/2}}\right) - \mathrm{erf}\left(\frac{s\sqrt{2} - z\psi\beta_z}{s^{1/2}}\right)\right] . \end{aligned} \tag{A8}$$

With that, Eq. A6 becomes

$$r(s) \approx \upsilon_z \frac{(1 + \kappa_z)}{\beta_z} I_1 \exp\left(s - 2z\psi\beta_z + \frac{(z\psi\beta_z)^2}{s}\right) \quad . \tag{A9}$$

Finally, by using $t_z = (1 - 2\beta_z)/(2\beta_z)$, the correction factor can be estimated as $\kappa_z \approx \sum_{k=2}^{\infty}(-1)^{k-1} t_z^{k-1} = -t_z/(1 + t_z) = 2\beta_z - 1$, so that $(1 + \kappa_z) \approx 2\beta_z$, and expression A9, together with the result A8, leads to our main result, *i.e.*, Eq. 7.

Appendix B: Work to form a n-sized cluster

Following the framework discussed in Refs.[13,16], we consider that the work to form a cluster with n particles can be written as

$$W(n) = -n\Delta\mu + \Phi(n) \quad , \tag{B1}$$

where $\Delta\mu = k_B T \ln(C_1/C_e)$, and

$$\Phi(n) = \psi k_B T l(n) \tag{B2}$$

is the effective excess energy, with $l(n)$ being the number of non-connected bonds at the periphery of the cluster, and $\psi = \sigma/k_B T$ is a dimensionless ratio defined in terms of the effective surface energy per particle σ (see, *e.g.*, Refs.[13,17]). Ideally, ψ should be proportional to the ratio $\omega = \varepsilon/2k_B T$ defined in KMC, where ε is the effective interaction energy[13]. However, at finite temperatures, ψ can be significantly lower than ω, and even close to zero as T goes to the critical temperature, *i.e.*, as ω goes to the corresponding critical ratio ω_c^z. In particular, for the lattices formed by the model particles defined here those values are estimated as[22] $\omega_c^4 = 0.88137$, $\omega_c^{5(c)} = 0.68346$, $\omega_c^{5(d)} = 0.69314$, and $\omega_c^6 = 0.54931$ (see the caption and the panel (e) in Fig. 4).

In general, the number of non-connected bonds at the periphery of the cluster can be written as[13]

$$l(n) = zn - 2g(n) \quad , \tag{B3}$$

with the term zn being the total number of bonds available for n particles with ligancy z, and $g(n)$ the number of bonds in the n-sized cluster. Importantly, the number of bonds can be used to define the effective interaction energy of the n-sized cluster as $E_b(n) = -\varepsilon g(n)$, with $\varepsilon = 2\omega k_B T$. Hence, in order to obtain $g(n)$ and $l(n)$, we consider that $n_b < n$ particles contribute with energy λ, and n_s particles, which are at the periphery of the cluster, contribute with energy $\lambda' < \lambda$, that is, $E_b(n) = -\lambda n_b - \lambda' n_s$. In addition, we assume that $n_s(n) = c_z(n^{\alpha} - 1)$, with $0 < \alpha \leq 1$ and $c_z > 0$ being a parameter that should dependent on the ligancy z. Since the condition $n_b = 0$ and $n_s = 0$ should be satisfied for $n = 1$, one must have that $n_b + n_s = n - 1$, hence $E_b(n) = -\lambda[(n-1) - (1 - \delta_z)c_z(n^{\alpha} - 1)]$, where it was assumed that $\lambda' = \delta_z\lambda$ with $\delta_z < 1$. Finally, by considering $(1 - \delta_z)c_z = \beta_z/\alpha$ and $\lambda = z\varepsilon/2$, with $\varepsilon = 2\omega k_B T$ being the effective binding energy[13], one can rewrite the total binding energy as $E_b(n) = -\varepsilon g(n)$, where the number of bonds in the n-sized cluster is

$$g(n) = \frac{z}{2}\left[(n-1) - \frac{\beta_z}{\alpha}(n^{\alpha} - 1)\right] \quad . \tag{B4}$$

Thus, by considering expression B3 for the number of non-connected bonds, Eq. B4 leads to

$$l(n) = z\left[1 + \frac{\beta_z}{\alpha}(n^{\alpha} - 1)\right] \quad . \tag{B5}$$

Accordingly, the above expressions generalise the results for the square (2D, $d = 2$) and cubic (3D, $d = 3$) regular lattices that are somewhat expected from a Kossel crystal (KC), see Ref.[13]. To retrieve those expected values, one can simply set $\alpha_{\rm KC} = (d-1)/d$, $\beta_{\rm KC} = \alpha_{\rm KC}$, and $z = 2d$, so that Eqs. B4 and B5 yield, respectively, $b_{\rm 2D}(n) = 2(n - n^{1/2})$ and $l_{\rm 2D}(n) = 4n^{1/2}$, for $d = 2$, and $b_{\rm 3D}(n) = 3(n - n^{2/3})$ and $l_{\rm 3D}(n) = 6n^{2/3}$, for $d = 3$.

Finally, by considering Eqs. B1 and B5, one has that the (dimensionless) work to form a cluster with n particles is given by

$$w(n) = \frac{W(n)}{k_B T} = -sn + \frac{z\psi\beta_z}{\alpha}(n^\alpha - 1) + z\psi \quad , \qquad \text{(B6)}$$

where $s = \Delta\mu/k_B T$ is the supersaturation. We note that Eq. 10 is obtained from the above equation by setting $\alpha = 1/2$. Additionally, one can use the condition of maximum work[13], $(dw(n)/dn)_{n=n^*-1} = 0$, to obtain the corrected estimate for the critical nucleus size, that is,

$$n^*(s) = \frac{Q_z}{s^\gamma} + 1 \qquad \text{(B7)}$$

with $Q_z = (z\psi\beta_z)^\gamma$ and $\gamma = 1/(1-\alpha)$. By choosing $\alpha = 1/2$ one has that $\gamma = 2$, which corresponds to Eq. 14 in the main text. In particular, the corrected expression for n^* for the two-dimensional Kossel crystal obtained in Ref.[13] can be recovered by assuming that $\beta_z = 1/2$.

REFERENCES

[1] G. Foffi and F. Sciortino, "On the possibility of extending the Noro-Frenkel generalized law of correspondent states to non-isotropic patchy interactions," J. Phys. Chem. B **111**, 9703 (2007).

[2] J. I. Urgel, D. Écija, G. Lyu, R. Zhang, C.-A. Palma, W. Auwärter, N. Lin, and J. V. Barth, "Quasicrystallinity expressed in two-dimensional coordination networks," Nature Chem. **8**, 657 (2016).

[3] A. J. Williamson, A. W. Wilber, J. P. K. Doye, and A. A. Louis, "Templated self-assembly of patchy particles," Soft Matter **7**, 3423 (2011).

[4] A. Reinhardt, C. P. Ho, and D. Frenkel, "Effects of co-ordination number on the nucleation behaviour in many-component self-assembly," Faraday Discuss. **186**, 21 (2016).

[5] D. Écija, J. I. Urgel, A. C. Papageorgiou, S. Joshi, W. Auwärter, A. P. Seitsonen, S. Klyatskaya, M. Ruben, S. Fischer, S. Vijayaraghavan, J. Reichert, and J. V. Barth, "Five-vertex Archimedean surface tessellation by lanthanide-directed molecular self-assembly," Proc. Natl. Acad. Sci. U.S.A. **110**, 6678 (2013).

[6] D. V. Talapin, E. V. Shevchenko, M. I. Bodnarchuk, X. Ye, J. Chen, and C. B. Murray, "Quasicrystalline order in self-assembled binary nanoparticle superlattices," Nature **461**, 964 (2009).

[7] M. N. van der Linden, J. P. K. Doye, and A. A. Louis, "Formation of dodecagonal quasicrystals in two-dimensional systems of patchy particles," J. Chem. Phys. **136**, 054904 (2012).

[8] A. Reinhardt, F. Romano, and J. P. K. Doye, "Computing phase diagrams for a quasicrystal-forming patchy-particle system," Phys. Rev. Lett. **110**, 255503 (2013).

[9] J. H. ter Horst and D. Kashchiev, "Determining the nucleation rate from the dimer growth probability," J. Chem. Phys. **123**, 114507 (2005).

[10] J. H. ter Horst and D. Kashchiev, "Rate of two-dimensional nucleation: Verifying classical and atomistic theories by Monte Carlo simulation," J. Phys. Chem. B **112**, 8614 (2008).

[11] R. Cabriolu, D. Kashchiev, and S. Auer, "Breakdown of nucleation theory for crystals with strongly anisotropic interactions between molecules," J. Chem. Phys. **137**, 204903 (2012).

[12] R. J. Bingham, L. G. Rizzi, R. Cabriolu, and S. Auer, "Communication: Non-monotonic supersaturation dependence of the nucleus size of crystals with anisotropically interacting molecules," J. Chem. Phys. **139**, 241101 (2013).

[13] D. Kashchiev, "Toward a better description of the nucleation rate of crystals and crystalline monolayers," J. Chem. Phys. **129**, 164701 (2008).

[14] D. Kashchiev and S. Auer, "Nucleation of amyloid fibrils," J. Chem. Phys. **132**, 215101 (2010).

[15] D. Kashchiev, "Interrelation between cluster formation time, cluster growth probability, and nucleation rate," J. Chem. Phys. **127**, 064505 (2007).

[16] D. Kashchiev, *Nucleation: Basic Theory with Applications* (Butterworth-Heinemann, Oxford, 2000).

[17] L. Onsager, "Crystal statistics. i. a two-dimensional model with an order-disorder transition," Phys. Rev. **65**, 117 (1944).

[18] L. G. Rizzi and S. Auer, "Amyloid fibril solubility," J. Phys. Chem B **119**, 14631 (2015).

[19] M. Tsvetanova, K. Sotthewes, and H. J. W. Zandvliet, "Free energy of domain walls and order-disorder transition in a triangular lattice with anisotropic nearest-neighbor interactions," Phys. Rev. E **102**, 032138 (2020).

[20] C. H. Yang and H. Qiu, "Theory of homogeneous nucleation: A chemical kinetic view," J. Chem. Phys. **84**, 416 (1986).

[21] C. Haas and J. Drenth, "The interaction energy between two protein molecules related to physical properties of their solution and their crystals and implications for crystal growth," J. Cryst. Growth **154**, 126 (1995).

[22] A. Codello, "Exact Curie temperature for the Ising model on Archimedean and laves lattices," J. Phys. A: Math. Theor. **43**, 385002 (2010).